

AD-A129 784

THE POST-PROCESSING APPROACH IN THE FINITE ELEMENT  
METHOD PART 3 A POSTER. (U) MARYLAND UNIV COLLEGE PARK  
LAB FOR NUMERICAL ANALYSIS I BABUSKA ET AL. JUN 83

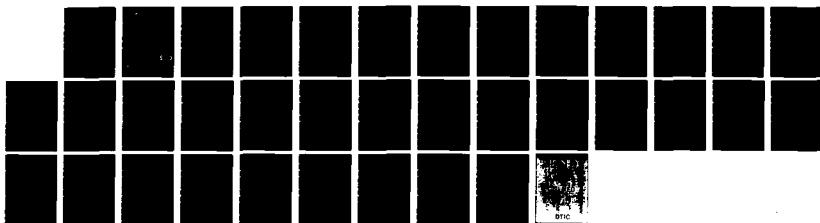
1/1

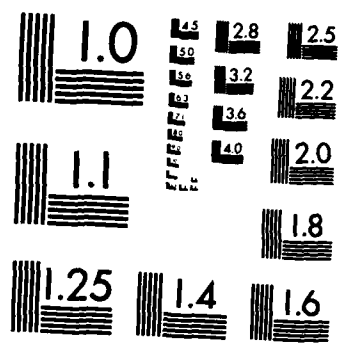
UNCLASSIFIED

BN-1007 N00014-77-C-0623

F/G 12/1

NL





MICROCOPY RESOLUTION TEST CHART  
NATIONAL BUREAU OF STANDARDS-1963-A



INSTITUTE FOR PHYSICAL SCIENCE  
AND TECHNOLOGY

13

ADA 1 29784

Laboratory for Numerical Analysis

Technical Note BN-1007

THE POST-PROCESSING APPROACH IN THE FINITE ELEMENT METHOD.

PART 3: A POSTERIORI ERROR ESTIMATES AND ADAPTIVE MESH SELECTION

by

I. Babuška and A. Miller

DTIC FILE COPY

DTIC  
ELECTE  
JUN 27 1983  
S D E

This document has been approved  
for public release and sale; its  
distribution is unlimited.

83 06 27 06 8

June 1983



UNIVERSITY OF MARYLAND

REPORT DOCUMENTATION PAGE		READ INSTRUCTIONS BEFORE COMPLETING FORM
1. REPORT NUMBER Technical Note BN-1007	2. GOVT ACCESSION NO. AD A129 714	3. RECIPIENT'S CATALOG NUMBER
4. TITLE (and Subtitle) THE POST-PROCESSING APPROACH IN THE FINITE ELEMENT METHOD. PART 3: A POSTERIORI ERROR ESTIMATES AND ADAPTIVE MESH SELECTION.		5. TYPE OF REPORT & PERIOD COVERED Final life of the contract
		6. PERFORMING ORG. REPORT NUMBER
7. AUTHOR(s) I. Babuška and A. Miller	8. CONTRACT OR GRANT NUMBER(s) ONR N00014-77-C-0623	
9. PERFORMING ORGANIZATION NAME AND ADDRESS Institute for Physical Science & Technology University of Maryland College Park, MD 20742		10. PROGRAM ELEMENT, PROJECT, TASK AREA & WORK UNIT NUMBERS
11. CONTROLLING OFFICE NAME AND ADDRESS Department of the Navy Office of Naval Research Arlington, VA 22217		12. REPORT DATE June 1983
		13. NUMBER OF PAGES 29
14. MONITORING AGENCY NAME & ADDRESS (if different from Controlling Office)		15. SECURITY CLASS. (of this report)
		15a. DECLASSIFICATION/DOWNGRADING SCHEDULE
16. DISTRIBUTION STATEMENT (of this Report)  Approved for public release: distribution unlimited		
17. DISTRIBUTION STATEMENT (of the abstract entered in Block 20, if different from Report)		
18. SUPPLEMENTARY NOTES		
19. KEY WORDS (Continue on reverse side if necessary and identify by block number)		
20. ABSTRACT (Continue on reverse side if necessary and identify by block number) This paper is the final in a series of three in which we have discussed a finite element post-processing technique. Here we shall deal with the questions of adaptive mesh selection and a posteriori error estimation. Some numerical examples computed by the FEARS program will be used to illustrate the approaches taken.		

Laboratory for Numerical Analysis

Technical Note BN-1007

THE POST-PROCESSING APPROACH IN THE FINITE ELEMENT METHOD  
PART 3: A POSTERIORI ERROR ESTIMATES AND ADAPTIVE MESH SELECTION

by

I. Babuška and A. Miller

Accession For	
NTIS GRA&I	<input checked="checked" type="checkbox"/>
DTIC TAB	<input type="checkbox"/>
Unannounced	<input type="checkbox"/>
Justification	
By	
Distribution/	
Availability Codes	
Dist	Avail and/or Special
A	



This research was partially supported by ONR Contract N00014-77-C-0623.  
The computations were carried out with support from the Computer Science  
Center at the University of Maryland, College Park.

# ABSTRACT

This paper is the final in a series of three in which we have discussed a finite element post-processing technique. Here we shall deal with the questions of adaptive mesh selection and a posteriori error estimation. Some numerical examples computed by the FEARS program will be used to illustrate the approaches taken.

## §1. Introduction

This is the final in a series of three papers in which we have sought to show how a suitable post-processing of a finite element solution can yield accurate pointwise values for quantities such as displacements, stresses, flow rates and stress intensity factors. In [1] and [2] we derived a number of extraction expressions for such quantities in the setting of some simple model problems, and saw how these expressions could serve as the bases of effective post-processing techniques. We also carried out an error analysis for such post-processing computations. This analysis showed that the accuracy of the post-processed value could be related to how well the space of finite element functions is able to approximate both the solution of the basic problem and the solution of a related auxiliary problem. This auxiliary problem is of the same form as the basic problem, though with different loading data. (See §2.5 and §3.4 of [1]; and §4 of [2].)

Hitherto, except for a few qualitative remarks, we have said little concerning the issues of

(i) choosing a finite element subspace for calculating the approximate solution which is to be subsequently post-processed;

(ii) estimating, a posteriori, the error in a computed post-processed value.

The significance of both (i) and (ii) is quite clear. In practice, the goal of any post-processing computation is to obtain a post-processed value of a specified accuracy at a minimal total computational cost. An estimate as in (ii) provides a means of determining when the specified accuracy has been attained, whereas the choice in (i) largely determines the efficiency of the overall numerical procedure.

In this paper we propose a post-processing algorithm. It is based on the extraction techniques of [1] and [2], and includes features that enable (i) and (ii) to be handled quite effectively. Our discussion will be in the context of the "membrane" model problems already introduced in §5 of [1] and §6 of [2]. In these the order of the elements employed is fixed (square bilinear elements are used), and (i) becomes a matter of choosing a finite element mesh (i.e., nodal points). The manner in which we realize (i) and (ii) will make use of some of the features available in the FEARS program. In §2 of this paper we briefly describe the relevant features of FEARS. In §3.1 we review the error analysis of our earlier papers [1] and [2] and show how this analysis suggests some a posteriori error estimates that can be computed within the FEARS framework. These a posteriori estimates are the basis of the proposed algorithm, which we describe in §3.2. Finally, in §4 we return to some of the numerical examples of §5 of [1] and §6 of [2], this time concentrating on some new aspects which are related to the issues (i) and (ii).



## §2. The FEARS program

FEARS is a research oriented, adaptive finite element code developed at the University of Maryland. A detailed description of the operation of the program can be found in [3]. For the purposes of this paper, the following few remarks will suffice. As already explained in [2], FEARS assumes that the region under consideration has firstly been partitioned into a number of subregions, each of which is a curvilinear quadrilateral. Within the program, each of these subregions is transformed by a change of coordinates into a unit square. The actual finite element modelling is carried out on these transformed squares. Square bilinear elements are used. FEARS has an adaptive character: starting from an initial coarse mesh (usually uniform on each of the transformed squares), the program automatically selects, in a recursive fashion, a sequence of "optimal" mesh refinements.

The mesh refinement procedure is based upon a set of non-negative error indicators. An indicator,  $\eta_{\Delta}$  say, is associated with each element  $\Delta$ . It is calculated only using information about the finite element solution on  $\Delta$  itself and on the immediately adjacent elements. These error indicators, when summed over all elements to obtain

$$(2.1) \quad \varepsilon = \sum_{\substack{\text{all elements} \\ \Delta}} \eta_{\Delta}$$

say, yield an estimate for some user specified measure of the error in the finite element solution. Typically, this measure is closely related to the energy of the error. (Later we shall say a little more. See [3

and §4.) Each step in the refinement process is directed towards minimizing the sum  $\epsilon$  of (2.1) in some "optimal" fashion. To this end, all elements  $\Delta$  of an existing mesh whose error indicators  $\eta_{\Delta}$  exceed a threshold value are subdivided. This threshold is determined from some information on the past history of the refinement process. Of course, the character of the meshes constructed by FEARS will depend upon which error measure has been specified. This reflects the fact that the quality of a mesh is not an absolute property, but must be viewed relative to the ultimate goal of the finite element calculation. We shall elaborate further upon the point in §4.

In FEARS the finite element equations are solved by a direct method. Usually, after each refinement step a full new solution is calculated and a new set of error indicators is found. However, calculating a new solution each time is quite expensive, and as it is just an intermediate step, only being used to compute the new error indicators for the next refinement step, one would like to avoid it, if possible. FEARS has a number of "economy" modes which do this to varying degrees. In these a full solution is computed only after a specified increase in the total number of elements has occurred since the last full solution. After any refinement step between two such full solution phases, the new error indicators are only approximated on the basis of the past history of the local refinement process. This "economy" mode permits a multi-level refinement to take place between two full solutions. This possibility is particularly desirable for efficient operation for problems with severe singularities. Provided the number of such "short passes" between full solution steps is not too great, the resulting refinement pattern does not

differ too much from that obtained by the all full solution method, but, of course, with a considerable saving in computational cost.

Estimates such as  $\epsilon$  of (2.1), as well as being the basis of the automatic mesh refinement feature of FEARS, also provide a means of a posteriori error estimation. Of course, we cannot expect that the estimate  $\epsilon$  should yield the exact value of the specified error measure. However, under suitable assumptions, estimates may be calculated that are asymptotically exact. That is, if  $e$  denotes the exact value of the desired error measure, then

$$e = \epsilon(1+o(1)) \quad \text{as } \epsilon \rightarrow 0.$$

To illustrate some of the points made above, let us return to Example A of §6 of [2]. In that example we considered the boundary value problem

$$\begin{aligned} \nabla^2 \omega &= 0 \quad \text{in } \Omega \\ \omega &= 0 \quad \text{on } \Gamma_1 \\ \frac{\partial \omega}{\partial n} &= 0 \quad \text{on } \Gamma_2 \\ \frac{\partial \omega}{\partial n} &= x_2 \quad \text{on } \Gamma_3, \end{aligned} \tag{2.2}$$

where  $\Omega$  is the unit circle slit along the positive  $x_1$  axis and  $\Gamma_1$ ,  $\Gamma_2$  and  $\Gamma_3$  are as shown in Fig. 1. In [2] we reported on a sequence of five adaptively refined meshes that FEARS constructed for this problem (see §6.2 of [2]). We can now be more specific. The mesh refinement process for this example relied upon error indicators  $\eta_\Delta$  for which the

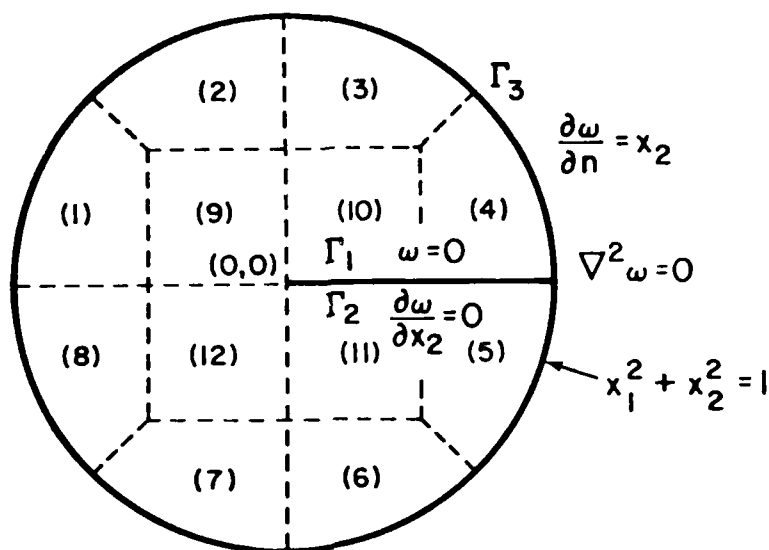


Figure 1

The region for the model problem (2.2)

sum  $\epsilon$  of (2.1) is an asymptotically exact estimate for the strain energy measure  $e = \int_{\Omega} |\nabla(\omega - \tilde{\omega})|^2 dA$  of the error in the finite element solution  $\tilde{\omega}$ . As we saw in [2], the meshes so constructed yield a rate of convergence for the strain energy norm  $e^{1/2}$  of the error that is close to the theoretically optimal rate of  $O(N^{-1/2})$ , where  $N$  is the number of degrees-of-freedom of the finite element model. In contrast, uniform meshes would only give an  $O(N^{-1/8})$  rate. In Table 1 we have listed  $e^{1/2}$  and  $\epsilon^{1/2}$  for each of our meshes. Notice the  $\frac{\epsilon^{1/2}}{e^{1/2}}$  appears to be converging to 1, as it should, since  $\epsilon$  is an asymptotically exact estimate for  $e$ . For this problem FEARS was executed in an "economy" mode, so permitting multi-level refinements between full solutions (the

meshes I-V that we have referred to here and in [2] are a selection of meshes created by full solution steps). The efficiency of the "economy" mode can be gauged by the fact that the total solution time for mesh V and all earlier full solutions was only about 2.5 times the solution time for mesh V alone.

MESH LABEL (degrees-of-freedom)	$e^{1/2}$ true error norm ( $e^{1/2}/E(w)^{1/2}$ )	$\epsilon^{1/2}$ estimated error norm	$\frac{1}{\sqrt{2}}$
I (56)	.6577 (30.9%)	.3747	.57
II (89)	.5156 (24.2%)	.3544	.69
III (118)	.3875 (18.2%)	.3108	.80
IV (171)	.2622 (12.3%)	.2434	.93
V (391)	.1618 ( 7.6%)	.1638	1.01

TABLE 1. A posteriori estimates of the error in the energy norm  $e^{1/2}$  for the example of §2. ( $E(w) = \int_{\Omega} |\nabla w|^2 dA$ ).

### §3.1. A Posteriori Error Estimates

For the model problems discussed in §5 of [1] and in [2] we saw that the difference between the exact value  $\phi$  of some quantity (e.g. displacement, stress, stress intensity factor) associated with the exact solution  $\omega$  of a problem and an approximate value  $\tilde{\phi}$  obtained by suitably post-processing the finite element solution  $\tilde{\omega}$  could be expressed as

$$(3.1) \quad \phi - \tilde{\phi} = \int_{\Omega} \nabla(\omega - \tilde{\omega}) \cdot \nabla(\psi - \tilde{\psi}) dA,$$

where  $\psi$  and  $\tilde{\psi}$  are the exact and finite element solutions respectively of an auxiliary problem. This auxiliary problem is of the same form as the basic problem for  $\omega$ , though with different loading data. The loading data is determined by the particular extraction functions used in the post-processing calculations.

For any function  $u$ , let  $E(u)$  denote the "membrane" strain energy of  $u$ ,

$$E(u) = \int_{\Omega} |\nabla u|^2 dA.$$

After a little algebraic manipulation (3.1) may be rewritten as

$$(3.2) \quad \phi - \tilde{\phi} = \frac{1}{4} [E((\omega + \psi) - (\tilde{\omega} + \tilde{\psi})) - E((\omega - \psi) - (\tilde{\omega} - \tilde{\psi}))].$$

Furthermore, the following inequalities also follow from (3.1),

$$(3.3a) \quad |\phi - \tilde{\phi}| \leq E(\omega - \tilde{\omega})^{1/2} E(\psi - \tilde{\psi})^{1/2},$$

$$(3.3b) \quad |\phi - \tilde{\phi}| \leq \frac{1}{2\alpha} (E(\omega - \tilde{\omega}) + \alpha^2 E(\psi - \tilde{\psi}))$$

for any real number  $\alpha > 0$ . Notice that whereas (3.2) is an exact expression for the error  $\phi - \tilde{\phi}$ , in general (3.3a) and (3.3b) only yield upper bounds for  $|\phi - \tilde{\phi}|$ . They fail to take account of any cancellation in the integral (3.1). The inequality (3.3a) becomes an equality only if  $(\omega - \tilde{\omega})$  and  $(\psi - \tilde{\psi})$  are multiples of one another. (The inequality (3.3b) is a equality only in the more particular case  $(\omega - \tilde{\omega}) = +\alpha(\psi - \tilde{\psi})$ .) One way to think of this cancellation phenomena is in terms of the "angle" between the errors  $(\omega - \tilde{\omega})$  and  $(\psi - \tilde{\psi})$ . Let  $\gamma$  be the angle lying between  $0^\circ$  and  $90^\circ$  for which

$$(3.4) \quad \cos \gamma = \frac{|\int_{\Omega} \nabla(\omega - \tilde{\omega}) \cdot \nabla(\psi - \tilde{\psi}) dA|}{E(\omega - \tilde{\omega})^{1/2} E(\psi - \tilde{\psi})^{1/2}}.$$

Then,  $\gamma = 0^\circ$  ( $\cos \gamma = 1$ ) corresponds to the case for which (3.3a) is an equality, while  $\gamma = 90^\circ$  ( $\cos \gamma = 0$ ) indicates complete cancellation in the integral (3.1). Continuing the geometrical analogy, we could say that in the case  $\gamma = 0^\circ$ , the errors  $(\omega - \tilde{\omega})$  and  $(\psi - \tilde{\psi})$  are "parallel," and in the case  $\gamma = 90^\circ$  they are "perpendicular."

Means of estimating the quantities appearing on the right hand sides of (3.2) and (3.3) are available in FEARS. If  $\tilde{u}$  is the finite element solution of a problem whose exact solution is  $u$ , let  $\epsilon^0(\tilde{u}) = \sum_{\Delta} \eta_{\Delta}^0(\tilde{u})$  be an asymptotically exact estimate for  $E(u - \tilde{u})$  which is constructed from elementary error indicators  $\eta_{\Delta}^0(\tilde{u})$ . That is,

$$E(u - \tilde{u}) = \epsilon^0(\tilde{u})(1 + o(1)) \quad \text{as } E(u - \tilde{u}) \rightarrow 0$$

So (3.2) gives,

$$(3.5) \quad \phi - \tilde{\phi} = \frac{1}{4} [\epsilon^0(\omega + \tilde{\psi}) - \epsilon^0(\omega - \tilde{\psi})] + o(1) [\epsilon^0(\tilde{\omega} + \tilde{\psi}) + \epsilon^0(\tilde{\omega} - \tilde{\psi})],$$

and (3.3) leads to

$$(3.6a) \quad |\phi - \tilde{\phi}| \leq \epsilon^0(\tilde{\omega})^{1/2} \epsilon^0(\tilde{\psi})^{1/2} (1+o(1))$$

$$(3.6b) \quad |\phi - \tilde{\phi}| \leq \frac{1}{2\alpha} (\epsilon^0(\tilde{\omega}) + \alpha^2 \epsilon^0(\tilde{\psi})) (1+o(1))$$

where the  $o(1)$  term is valid as  $E(\omega - \tilde{\omega}) + E(\psi - \tilde{\psi}) \rightarrow 0$ .

The equation (3.5) suggests that the quantity

$$(3.7) \quad \epsilon_1 = \frac{1}{4} [\epsilon^0(\tilde{\omega} + \tilde{\psi}) - \epsilon^0(\tilde{\omega} - \tilde{\psi})]$$

should provide a good estimate for the error  $\phi - \tilde{\phi}$  provided the  $o(1)$  term is negligible. However, if the  $o(1)$  term in (3.5) is comparable

to  $\mu = \frac{\frac{1}{4} [\epsilon^0(\tilde{\omega} + \tilde{\psi}) - \epsilon^0(\tilde{\omega} - \tilde{\psi})]}{\epsilon^0(\tilde{\omega} + \tilde{\psi}) + \epsilon^0(\tilde{\omega} - \tilde{\psi})}$  then  $\epsilon_1$  is no longer reliable. In cases

where the angle  $\gamma$  defined in (3.4) is close to  $90^\circ$ , then  $\mu$  may be quite small and  $\epsilon_1$  could well perform poorly. Turning now to (3.6), we see that, at least asymptotically, the quantities

$$(3.8a) \quad \epsilon_2 = \epsilon^0(\tilde{\omega})^{1/2} \epsilon^0(\tilde{\psi})^{1/2}$$

$$(3.8b) \quad \epsilon_3 = \frac{1}{2\alpha} (\epsilon^0(\tilde{\omega}) + \alpha^2 \epsilon^0(\tilde{\psi}))$$

give upper bounds for  $|\phi - \tilde{\phi}|$ . From what we have said before it can be seen that the extent of the asymptotic overestimation of  $|\phi - \tilde{\phi}|$  by  $\epsilon_2$  is closely related to the angle  $\gamma$ . For  $\gamma$  near  $0^\circ$ ,  $\epsilon_2$  is



asymptotically a very sharp estimate for  $|\phi - \tilde{\phi}|$ , whereas if  $\gamma$  is close to  $90^\circ$ ,  $\epsilon_2$  will be a considerable overestimate.

### 3.2. The Numerical Algorithm

Let us now briefly list some features of the algorithm that we mentioned in the Introduction:

(a) Instead of only solving for  $\tilde{\omega}$ , solutions for both  $\tilde{\omega}$  and  $\tilde{\psi}$  are calculated. This is not as labourious as it may at first seem, since the auxiliary problem for  $\psi$  and the basic problem for  $\omega$  differ only in their loading data. Thus, they may be thought of as the solutions of a multiple load problem.

(b) The pair of solutions  $\tilde{\omega}$  and  $\tilde{\psi}$  are computed for a sequence of adaptively refined meshes using the FEARS program. The mesh refinement steps are based on the particular choice of error indicators

$$(3.9) \quad \eta_{\Delta} = \frac{1}{2\alpha}(\eta^0(\tilde{\omega}) + \alpha^2 \eta_{\Delta}^0(\tilde{\psi}))$$

where  $\alpha > 0$  is some user chosen constant. The choice (3.9) is obviously suggested by (3.6b). The logic being that with this choice the adaptive mesh refinement process is directed by an "optimal" minimization of the estimate  $\epsilon_3$ . Recall that asymptotically  $\epsilon_3$  is, in general, only an upper bound for  $|\phi - \tilde{\phi}|$ , the degree of overestimation being determined by, amongst other factors, the angle  $\gamma$  and the value of  $\alpha$ . It would seem preferable to employ error indicators whose sum provided a sharper estimate than (3.6b). Unfortunately, the two other estimates  $\epsilon_1$  and  $\epsilon_2$  that we have available cannot be expressed in the form (2.1). In the case of  $\epsilon_1$ , choosing  $\eta_{\Delta} = \frac{1}{4}(\eta^0(\tilde{\omega} + \tilde{\psi}) - \eta_{\Delta}^0(\tilde{\omega} - \tilde{\psi}))$  would not always ensure that  $\eta_{\Delta} \geq 0$ . The estimate  $\epsilon_2$  cannot be conveniently written as an element by element sum, though by a proper choice of  $\alpha$  the values

of  $\epsilon_2$  and  $\epsilon_3$  can be made close. We shall say a little more about this later.

(c) Although  $\epsilon_1$  and  $\epsilon_2$  cannot be used in the role described in (b), they can still nonetheless be computed as global quantities and be employed as a posteriori error estimates. As such, they provide a means of stopping the mesh refinement process once sufficient accuracy has been attained. Of course,  $\epsilon_1$  would provide a superior estimate to  $\epsilon_2$  as long as the above-mentioned loss of reliability associated with angles  $\gamma$  near  $90^\circ$  does not occur.

#### §4. Numerical Examples

##### §4.1. The membrane Examples of §5 of [1]

Let us reconsider the example that we first discussed in §5 of [1].  
In that example we dealt with the boundary value problem.

$$(4.1) \quad \begin{aligned} \nabla^2 \omega &= -1 \quad \text{in } \Omega = (-1,1)^2 \\ \omega &= 0 \quad \text{on the boundary } \partial\Omega \text{ of } \Omega. \end{aligned}$$

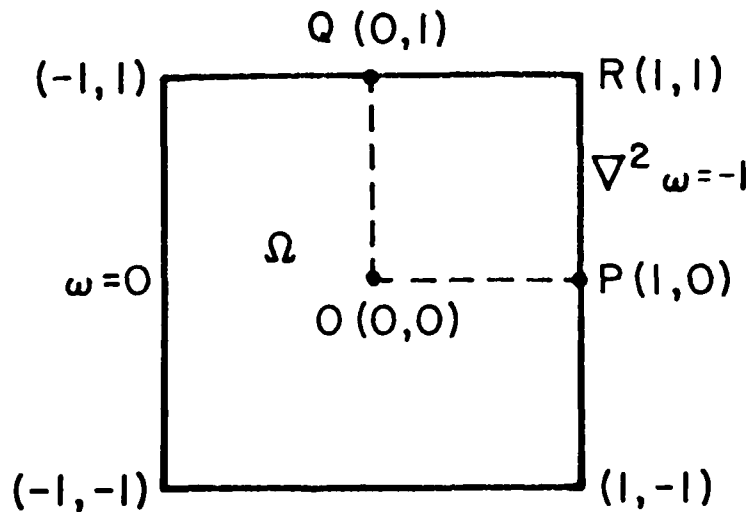


Figure 2

The region for for the model problem (4.1)

One of our goals in that example was to find approximate values for the "stress"  $\phi_2 = \frac{\partial u}{\partial x_1}$  at  $P(1,0)$  (see Fig. 2). In [1] we presented three different extraction expressions for this stress. These extraction expressions differed in the way that they handled the boundary conditions for the generating function. Here we shall only further discuss the case (c) of §5.3 of [1]; that is, we consider post-processing calculations based on the extraction expression

$$(4.2) \quad \tilde{\phi}_2(\tilde{\omega}) = \int_{\Omega} \nabla^2 \tilde{\phi} \tilde{\omega} dA + \int_{\Omega} \tilde{\phi} dA$$

where

$$\tilde{\phi} = \frac{1}{\pi} \left[ \frac{(x_1-1)}{(x_1-1)^2 + x_2^2} - \left\{ \frac{x_1-1}{(x_1-1)^2 + 1} + \frac{x_1-1}{4+x_2^2} - \frac{x_1-1}{5} \right\} \right].$$

The auxiliary problem associated with (4.2) is

$$(4.3) \quad \begin{aligned} \nabla^2 \psi &= -\nabla^2 \tilde{\phi} \quad \text{in } \Omega \\ \psi &= 0 \quad \text{on } \partial\Omega, \end{aligned}$$

which, as it should be, is of the same form as (4.1) but with different right hand sides.

In [1] we saw that (4.2) led to highly accurate approximations for  $\phi_2$ , even in the case of quite coarse meshes. The numerical results we reported there were for a sequence of uniform meshes. At the time we did not comment on this particular selection of meshes. Qualitatively however, such a choice would not seem unreasonable from the viewpoint of

the theory we developed in [1] and [2]. The solutions of both the basic problem (4.1) and the auxiliary problem (4.3) are relatively smooth. Thus, uniform meshes would seem appropriate. In fact, the adaptive mesh refinement algorithm that we outlined in §3.2 exactly reproduces this sequence of meshes, independently of  $\alpha$ .

Using the estimates given in §3.1 we are able to estimate the error in the post-processed value  $\tilde{\Phi}_2$ . For the above meshes, Table 2 lists a selection of a posteriori estimates for  $|\Phi_2 - \tilde{\Phi}_2|$  based on (3.7) and (3.8). Notice that in the case of  $\epsilon_1$  the ratio of the estimated error to the true error in  $\tilde{\Phi}_2$  appears to converge to 1 as the mesh size is decreased. This is consistent with (3.5). On the other hand, for  $\epsilon_2$  and  $\epsilon_3$  the corresponding ratios each seem to stabilize around values greater than 1 as the mesh is refined. Again, this is expected on the basis of (3.6) which shows that  $\epsilon_2$  and  $\epsilon_3$  will, in general, asymptote to upper bounds for the error. Let us also remark that since  $\epsilon_2$  gives only a slight overestimation of  $|\Phi_2 - \tilde{\Phi}_2|$  and  $\epsilon_1$  behaves quite well, we should expect that the angle  $\gamma$  between  $(\omega - \tilde{\omega})$  and  $(\psi - \tilde{\psi})$  is not too close to  $90^\circ$ . In Table 2 we have listed an estimate for this angle which confirms this expectation. Notice also the interesting fact that  $\gamma$  is almost independent of the mesh.

No. of elements in quarter segment (uniform mesh)	4	16	64
$ \phi_2 - \frac{\partial \tilde{\omega}}{\partial x_1}(P)  /  \phi_2 $ relative error in standard finite element stress value	29%	16%	8.7%
$ \phi_2 - \tilde{\phi}_2 $ error in post-processed stress value $( \phi_2 - \tilde{\phi}_2  /  \phi_2 )$	10.495(-3) (1.5%)	2.553(-3) (.37%)	0.637(-3) (.089%)
$\gamma$ angle between $(\omega - \tilde{\omega})$ and $(\psi - \tilde{\psi})$ (see (3.4))	37.1°	37.0°	38.6°
$\epsilon_j$ estimated error $(\epsilon_j /  \phi_2 - \tilde{\phi}_2 )$			
$\epsilon_1$	10.351(-3) (.986)	2.599(-3) (1.018)	0.641(-3) (1.006)
$\epsilon_2$	12.976(-3) (1.236)	3.255(-3) (1.275)	0.820(-3) (1.287)
$\epsilon_3$	24.412(-3) (2.326)	6.444(-3) (2.524)	1.689(-3) (2.651)

TABLE 2. A posteriori estimates of the error in  $\tilde{\phi}_2$  for the example discussed in §4.1.  $\epsilon_1 = \frac{1}{4} |\epsilon^0(\tilde{\omega} + \tilde{\psi}) - \epsilon^0(\tilde{\omega} - \tilde{\psi})|$ ,  $\epsilon_2 = \epsilon^0(\tilde{\omega})^{1/2} \epsilon^0(\tilde{\psi})^{1/2}$ ,  $\epsilon_3 = \frac{1}{2} (\epsilon^0(\tilde{\omega}) + \epsilon^0(\tilde{\psi}))$ .

#### §4.2. The Slit Membrane Example of §6.2 of [2]

In this section we shall return to Example A of §6 of [2]. We have already used this example in §2 of this paper to illustrate some of the features of the FEARS program. The governing equations and boundary conditions are given in (2.2) and depicted in Fig. 1. As in [2], let us be interested in using post-processing techniques to find approximations to the leading stress intensity factor  $k_1$ . Recall that  $k_1$  was defined to be the coefficient of the leading term in the asymptotic expansion

$$(4.4) \quad \omega = k_1 r^{1/4} \sin \frac{\theta}{4} + O(r^{3/4}) \quad (k_1 = 1.35812)$$

for  $\omega$  in the vicinity of the slit tip  $(0,0)$ . Here we shall only treat post-processing calculations based upon the extraction expression

$$(4.5) \quad \tilde{k}_1 = \int_{\Gamma_3} (x_2 \phi - \nabla \phi \cdot \hat{n} \tilde{\omega}) ds$$

where

$$\phi = \frac{2}{\pi} r^{-1/4} \sin \frac{\theta}{4}.$$

The expression (4.5) is an instance of what we have been calling a generalized influence function method. The auxiliary function introduced in the error analysis of the extraction expression (4.5) is

$$(4.6) \quad \begin{aligned} \nabla^2 \psi &= 0 && \text{in } \Omega \\ \psi &= 0 && \text{on } \Gamma_1 \\ \frac{\partial \psi}{\partial \mathbf{n}} &= 0 && \text{on } \Gamma_2 \\ \frac{\partial \psi}{\partial \mathbf{n}} &= -\frac{\partial \phi}{\partial \mathbf{n}} && \text{on } \Gamma_3 \end{aligned}$$



By chance, in this case, we can explicitly solve (4.6) to obtain

$$(4.7) \quad \psi = \frac{2}{\pi} r^{1/4} \sin \frac{\theta}{4},$$

which is just a multiple of the leading term in the expansion (4.4) of  $\omega$ . (Of course, we cannot expect to be able to do this so simply in general.)

As explained in §2, the meshes we considered there and in [2] for this problem were constructed by FEARS using the error indicator  $\eta_{\Delta} = \eta_{\Delta}^0(\tilde{\omega})$ . (That is, on the basis of minimizing the estimate  $\epsilon^0$  of the strain energy  $E(\omega - \tilde{\omega})$  of the error.) Strictly speaking, this indicator does not fit into the framework we outlined in (b) of §3.2; though, it can be thought of as a limiting case as  $\alpha \rightarrow 0$ . However, executing the algorithm of §3.2 with a number of choices of  $\alpha$  leads to sequences of meshes which, though different from those above, show much the same refinement characteristics. For this reason, and since we want our numerical results here to complement those of [2], we shall work with the same sequence of meshes constructed for this problem in [2].

To try to see why the character of the meshes constructed above should be independent of  $\alpha$  let us rewrite (4.4) as

$$(4.8) \quad \begin{aligned} \omega &= k_1 r^{1/4} \sin \frac{\theta}{4} + \omega_0 \\ &= k_1 \frac{\pi}{2} \psi + \omega_0 \end{aligned}$$

where  $\omega_0 = O(r^{3/4})$ . Let  $\tilde{\omega}_0$  be the finite element solution that would be obtained were the loading in (2.2) such that  $\omega_0$  was the exact solution. By the linearity of the model problem,

$$\tilde{\omega} = k_1 \frac{\pi}{2} \tilde{\psi} + \tilde{\omega}_0$$

and consequently

$$(4.9) \quad \omega - \tilde{\omega} = k_1 \frac{\pi}{2} (\psi - \tilde{\psi}) + \omega_0 - \tilde{\omega}_0.$$

The function  $\omega_0$  is relatively smooth in comparison with  $\psi$ , however, from our point of view the relative magnitude of the factor  $k_1 \frac{\pi}{2}$  is equally important. If it is sufficiently large, then  $\frac{k_1 \pi}{2} (\psi - \tilde{\psi})$  will make the major contribution to the error  $\omega - \tilde{\omega}$ ; while if it is small enough, then for meshes that are not too fine, the  $\omega_0 - \tilde{\omega}_0$  contribution will dominate. As long as the first case applies, then an "ideal" finite element mesh would exhibit a severe refinement about the slit tip at (0,0), while if the latter case applies a more uniform mesh is called for, at least to begin with. Which case actually occurs in this problem is clearly demonstrated by the results shown in Table 3—for the level of refinement encountered there the  $\omega_0 - \tilde{\omega}_0$  contribution is relatively small. It is not surprising then, that regardless of whether the mesh refinement process is directed towards minimizing  $E(\omega - \tilde{\omega})$ ,  $E(\psi - \tilde{\psi})$  or some combination  $E(\omega - \tilde{\omega}) + \alpha^2 E(\psi - \tilde{\psi})$ , the resulting meshes will not be significantly different. However, we should point out, and the trend in Table 3 shows this, that at some point the magnitude of the two components in (4.9) will become comparable. At that point, the different choices of  $\alpha$  will lead to meshes of significantly different natures.

Mesh Label	$\frac{ k_1 \frac{\pi}{2}  E(\psi - \tilde{\psi})^{1/2}}{E(\omega - \tilde{\omega})^{1/2}}$	$\frac{E(\omega_0 - \tilde{\omega}_0)^{1/2}}{E(\omega - \tilde{\omega})^{1/2}}$
I	.98	.21
II	1.02	.22
III	.99	.25
IV	.96	.34
V	.94	.38

TABLE 3. Magnitude of the  $k_1 \frac{\pi}{2} (\psi - \tilde{\psi})$  and  $(\omega_0 - \tilde{\omega}_0)$  components of the error  $(\omega - \tilde{\omega})$ .

In Table 4 we list a number of different a posteriori estimates of the error in  $\tilde{k}_1$  for the above sequence of meshes, along with the exact values of the error and the angle  $\gamma$  which are able to be found analytically for this particular problem. The apparent asymptotic exactness of  $\epsilon_1$  is consistent with (3.5) and the fact that the angle  $\gamma$  is rather small. The estimates  $\epsilon_2$  and  $\epsilon_3$  appear to lead to upper bounds for  $|k_1 - \tilde{k}_1|$ . Since the angle  $\gamma$  is near  $0^\circ$  we would expect that  $\epsilon_2$  would, in the limit, give only a slight overestimation of the error. Again the numerical results in Table 4 are consistent with this.

Mesh Label (degrees-of-freedom)	I (56)	II (89)	III (118)	IV (171)	V (391)
$ k_1 - \tilde{k}_1 $ error in post-processed stress intensity factor $( k_1 - \tilde{k}_1  /  k_1 )$	.193860 (14.3%)	.123570 (9.1%)	.067090 (4.9%)	.029140 (2.1%)	.010690 (.79%)
$\gamma$ angle between $(\omega - \tilde{\omega})$ and $(\psi - \tilde{\psi})$ (see (3.4))	12.0°	12.5°	14.6°	20.1°	22.4°
$\epsilon_j$ estimated error $(\epsilon_j /  k_1 - \tilde{k}_1 )$					
$\epsilon_1$	.054270 (.28)	.055086 (.45)	.039720 (.59)	.022281 (.76)	.010163 (.95)
$\epsilon_2$	.059839 (.31)	.059906 (.48)	.043795 (.65)	.025825 (.89)	.011576 (1.08)
$\epsilon_3$	.082962 (.43)	.077077 (.62)	.058214 (.87)	.035249 (1.21)	.015912 (1.49)

TABLE 4. A posteriori error estimates for  $|k_1 - \tilde{k}_1|$  for the example of §4.2.

$$\epsilon_1 = \frac{1}{4} |\epsilon^0(\tilde{\omega} + \tilde{\psi}) - \epsilon^0(\tilde{\omega} - \tilde{\psi})|, \quad \epsilon_2 = \epsilon^0(\tilde{\omega})^{1/2} \epsilon^0(\tilde{\psi})^{1/2},$$

$$\epsilon_3 = \frac{1}{2} (\epsilon^0(\tilde{\omega}) + \epsilon^0(\tilde{\psi})).$$

#### §4.3. A Modification of the Slit Membrane Example of §6.2 of [2]

Let us now alter the basic problem (2.2) that we have been considering in §4.2 by modifying the loading so as to reduce the leading stress intensity factor by an order of magnitude or so. Specifically, in place of (2.2) consider

$$\begin{aligned}
 \nabla^2 \omega^* &= 0 \quad \text{in } \Omega \\
 \omega^* &= 0 \quad \text{on } \Gamma_1 \\
 \frac{\partial \omega^*}{\partial n} &= 0 \quad \text{on } \Gamma_2 \\
 \frac{\partial \omega^*}{\partial n} &= x_2 + \frac{1}{4} (1.3 \sin \frac{\theta}{4}) \quad \text{on } \Gamma_3
 \end{aligned}
 \tag{4.10}$$

which has the exact solution  $\omega^* = \omega + 1.3 r^{1/4} \sin \frac{\theta}{4}$ , where  $\omega$  is the solution of (2.2). The leading stress intensity factor for  $\omega^*$  is

$$k_1^* = k_1 + 1.3 = -.058122.$$

The algorithm §3.2 was executed for this problem with the following three different choices of error indicator  $\eta_\Delta$  of (3.9) governing the mesh construction process:

- (A)  $\eta_\Delta = \eta_\Delta^0(\tilde{\omega}^*)$  (This can be thought of as a limiting form of (3.9) as  $\alpha \rightarrow 0$ , the normalizing factor  $\frac{1}{2\alpha}$  of (3.9) having no effect on the refinement process.)
- (B)  $\eta_\Delta = \frac{\sqrt{5}}{2} (\eta_\Delta^0(\tilde{\omega}^*) + \frac{1}{5} \eta_\Delta^0(\tilde{\psi}))$
- (C)  $\eta_\Delta = \eta_\Delta^0(\tilde{\psi})$ . (This can be thought as a limiting form of (3.9) as  $\alpha \rightarrow \infty$ .)

Mesh Label	# of elements	# of d-o-f	Distribution of elements		$\Delta_A$	$\Delta_B$	$\Delta_C$	$\frac{k_1^* - k_1}{k_1^*}$
			inner	outer				
I*: (Initial uniform mesh)	48	46	25%	75%	7.98%	11.0%	53.4%	14.4%
II*: Strategy A, II* <sub>A</sub> Strategy B, II* <sub>B</sub> Strategy C, II* <sub>C</sub>	108	109	48%	52%	5.52%	8.53%	46.1%	4.22%
	123	117	55%	45%	5.08%	7.87%	42.5%	3.85%
	108	102	70%	30%	5.89%	7.78%	36.2%	3.15%
III*: Strategy A, III* <sub>A</sub> Strategy B, III* <sub>B</sub> Strategy C, III* <sub>C</sub>	339	330	45%	55%	2.37%	4.95%	30.6%	2.87%
	369	339	60%	40%	2.94%	4.03%	19.6%	1.23%
	396	323	92%	8%	5.42%	5.78%	15.2%	1.30%

TABLE 5. Properties of meshes for (4.10), refined using strategies A, B and C (see text for details).

Columns headed "Distribution of elements" list percentage of elements in subregions 9-12 (inner) and 1-8 (outer), see Fig. 1; d-o-f = degrees-of-freedom:

$$\Delta_A = \left( \frac{E(\omega^* - \tilde{\omega}^*)}{E(\omega^*)} \right)^{1/2}, \quad \Delta_B = \left( \frac{E(\omega^* - \tilde{\omega}^*) + \frac{1}{5} E(\psi - \psi^*)}{E(\omega^*) + \frac{1}{5} E(\psi)} \right)^{1/2}, \quad \Delta_C = \left( \frac{E(\omega^* - \tilde{\omega}^*)}{E(\omega^*)} \right)^{1/2}$$

Some numerical results for a selection of meshes obtained using each of these indicators is reported in Table 5. The first thing to notice from Table 5 is the very significant differences between the meshes created using each of the above three indicators. As the "distribution of elements" columns show, strategy (C) leads to meshes that concentrate elements in the inner subregions near the slit tip, while (B) and (A) produce progressively less severe refinement. This effect can be readily explained: In place of (4.9) we now have,

$$(4.11) \quad \omega^* - \tilde{\omega}^* = k_1^* \frac{\pi}{2} (\psi - \tilde{\psi}) + (\omega_0 - \tilde{\omega}_0),$$

and since  $|k_1^*|$  is now significantly smaller than  $|k_1|$ , we can no longer regard the  $(\omega_0 - \tilde{\omega}_0)$  contribution to the error as negligible, as we could in §4.2. Indeed, for the initial uniform mesh  $I^*$ , from which each of our strategies (A), (B) and (C) starts,

$$\frac{|k_1^* - \frac{\pi}{2}| E(\psi - \tilde{\psi})^{1/2}}{E(\omega^* - \tilde{\omega}^*)^{1/2}} = .20 \quad \text{and} \quad \frac{E(\omega_0 - \tilde{\omega}_0)^{1/2}}{E(\omega^* - \tilde{\omega}^*)^{1/2}} = .98$$

which is almost an exact reversal of the situation for mesh  $I$  in §4.2 (see Table 3). Therefore, it is to be expected that strategy (A), which seeks to minimize  $E(\omega^* - \tilde{\omega}^*)$ ; strategy (B), which seeks to minimize  $\frac{\sqrt{5}}{2} (E(\omega^* - \tilde{\omega}^*) + \frac{1}{5} E(\psi - \tilde{\psi}))$ ; and strategy (C), which seeks to minimize  $E(\psi - \tilde{\psi})$ , will now lead to meshes that are of a quite different nature from the very start. The meshes produced by (C) should exhibit the severest refinement, reflecting the fact that such a refinement is necessary to approximate the singular function  $\psi$  well. On the other

hand, (A) should produce the most uniform-like mesh, since early on, the smooth component  $\omega_0 - \tilde{\omega}_0$  dominates the error  $(\omega^* - \tilde{\omega}^*)$ , and uniform-like meshes are sufficient to approximate  $\omega_0$  well. The actual meshes produced are in accord with these expectations.

Notice also that the meshes produced by the algorithm seem to have achieved their respective goals in some "optimal" fashion, at least in comparison to one another. Among the meshes  $III_A^*$ ,  $III_B^*$  and  $III_C^*$ , each of which has a comparable number of degrees-of-freedom, the mesh  $III_A^*$  has the lowest value for  $E(\omega^* - \tilde{\omega}^*)$  (see column headed  $\Delta_A$ ), the mesh  $III_B^*$  has the lowest value for  $\frac{\sqrt{5}}{2} (E(\omega^* - \tilde{\omega}^*) + \frac{1}{5} E(\psi - \tilde{\psi}))$  (see column headed  $\Delta_B$ ), while the mesh  $III_C^*$  has the smallest energy error in  $(\psi - \tilde{\psi})$  (see column headed  $\Delta_C$ ).

Let us now turn to the accuracy in the post-processed value  $\tilde{k}_1^*$  for the various meshes. As we have said previously, this accuracy is dependent not only on the accuracy of  $\tilde{\omega}^*$  but also on the accuracy of  $\tilde{\psi}$ . Referring to Table 5, we see that the meshes  $II_A^*$  and  $III_A^*$ , though yielding good accuracies for  $\tilde{\omega}^*$  in the energy, are the worst members from among the sets  $II^*$  and  $III^*$  respectively as far as the accuracy of  $\tilde{\psi}^*$  in energy is concerned. Not surprisingly then, the accuracy of  $\tilde{k}_1^*$  for the meshes  $II_A^*$  and  $III_A^*$  is inferior to that for the corresponding meshes constructed using strategies (B) and (C). The question obviously arises as to what is the choice of  $\alpha$  for use in (3.9) that gives the best accuracy in  $\tilde{k}_1^*$  for a given number of degrees-of-freedom. This is a difficult matter to analyse in detail, though the results of Table 5 seem to indicate that, at least for this problem, the results are rather insensitive to non-zero choices of  $\alpha$ . As a rough guide though, and this is how we chose our



$\alpha = \frac{1}{\sqrt{5}}$ ,  $\alpha$  could be selected so that for the initial uniform mesh,  $\epsilon^0(\tilde{\omega}^*)$  and  $\alpha^2 \epsilon^0(\tilde{\psi})$  are about equal. The logic behind this choice being that this  $\alpha$  approximately equalizes  $\epsilon_3$  and the asymptotically sharper estimate  $\epsilon_2$  (at least for the initial uniform mesh). Although we had no need to do so in our calculations, one could possibly change  $\alpha$  during the course of the calculations to ensure that  $\epsilon_3$  and  $\epsilon_2$  always remain close to one another.

Finally, let us say a little about the a posteriori estimates for  $|k_1^* - \tilde{k}_1^*|$  based upon  $\epsilon_1$ ,  $\epsilon_2$  and  $\epsilon_3$ . Some numerical results for the mesh sequence I\*, II\*\_B and III\*\_B are reported in Table 6. We also list the value of the angle  $\gamma$  between the errors  $(\omega^* - \tilde{\omega}^*)$  and  $(\psi - \tilde{\psi})$ . For this problem we are able to calculate  $\gamma$  exactly. Notice that these angles are rather close to the critical value  $\gamma = 90^\circ$ . As we explained in §3.1, for such values of  $\gamma$  we expect the estimate  $\epsilon_1$  to be unreliable due to the significance of the second term of (3.5). In addition, the estimate  $\epsilon_2$  should be a considerable overestimation of  $|k_1^* - \tilde{k}_1^*|$ . Our numerical results seem to confirm both these points.

In general of course, we cannot calculate  $\gamma$ , and so in a case such as the above we could, just on the basis of  $\epsilon_1$ , be deceived into believing that there is greater accuracy in  $\tilde{k}_1^*$  than is actually the case. However, the fact that  $\epsilon_1$  and  $\epsilon_2$  differ by an order of magnitude or so should act as a warning that we are more than likely in a near critical case. (In fact, the ratio  $\frac{\epsilon_1}{\epsilon_2}$  is an estimate for  $\cos \gamma$ .) In such a situation,  $\epsilon_1$  should not be trusted, while  $\epsilon_2$  could be used to gauge the accuracy of  $\tilde{k}_1^*$ , realizing however, that it is probably a considerable overestimation of the error.

Mesh Label (degrees-of-freedom)	$I^*$ (56)	$II_B^*$ (117)	$III_B^*$ (339)
$ k_1^* - \tilde{k}_1^* $ error in post-processed stress intensity factor $  (k_1^* - \tilde{k}_1^*) /  k_1^*  )$	.8357(-2) (14.4%)	.2239(-2) (3.85%)	.0717(-2) (1.23%)
$\hat{r}$ angle between $(\omega^* - \tilde{\omega}^*)$ and $(\psi - \tilde{\psi})$ (see (3.4))	78.5°	84.0°	82.8°
$\epsilon_j$ estimated error $(\epsilon_j /  k_1^* - \tilde{k}_1^* )$			
$\epsilon_1$	.2360(-2) (.28)	.1566(-2) (.70)	.0103(-2) (.14)
$\epsilon_2$	1.7513(-2) (2.10)	1.4005(-2) (6.26)	.5170(-2) (7.21)
$\epsilon_3$	1.9150(-2) (2.29)	1.4042(-2) (6.27)	.5174(-2) (7.22)

TABLE 6. A posteriori estimates for  $|k_1^* - \tilde{k}_1^*|$  for the example of §4.3.

$$\epsilon_1 = \frac{1}{4} |\epsilon^0(\tilde{\omega}^* + \tilde{\psi}) - \epsilon^0(\tilde{\omega}^* - \tilde{\psi})|, \quad \epsilon_2 = \epsilon^0(\tilde{\omega}^*)^{1/2} \epsilon^0(\tilde{\psi}),$$

$$\epsilon_3 = \frac{\sqrt{5}}{2} (\epsilon^0(\tilde{\omega}^*) + \frac{1}{5} \epsilon^0(\tilde{\psi})).$$

### §5. Concluding Remarks

Our main intention in this paper was to examine the behaviour of the algorithm of §3.2 in some model post-processing applications, concentrating especially on the mesh selection and error estimation features of the algorithm. As far as accuracy of the post-processed value was concerned, the particular examples dealt with here proved rather insensitive to the choice of  $\alpha$  in the error indicator (3.9). In our most extreme example the spread in accuracy for the same number of degrees-of-freedom, was only by a factor of 2. Whether this insensitivity is a property to be expected in general is an open question at the moment. However, we can at least say from a theoretical point of view that some dependence on  $\alpha$  is to be expected whenever the basic and auxiliary problems have solutions with different "smoothness" characteristics.

Our examples also show that, except for the critical case when  $\gamma$  is near  $90^\circ$ , the error estimates  $\epsilon_1$  and  $\epsilon_2$  perform well asymptotically. The occurrence of the critical case can be detected numerically by the fact that  $\frac{\epsilon_2}{\epsilon_1} \geq 5$ , say. In this critical case, even though  $\epsilon_1$  appears unreliable,  $\epsilon_2$  still seems to provide a useable estimate, albeit an overly pessimistic one.

References

- [1] I. Babuška, A. Miller, The Post-Processing Approach in the Finite Element Method, Part 1: Calculation of Displacements, Stresses and other Higher Derivatives of Displacements, to appear in International Journal of Numerical Methods in Engineering.
- [2] \_\_\_\_\_, The Post-Processing Approach in the Finite Element Method, Part 2: The Calculation of Stress Intensity Factors, submitted to International Journal of Numerical Methods in Engineering.
- [3] C. Mesztenyi, W. Szymczak, FEARS User's Manual, Technical Note No. BN-991, 1982, Institute for Physical Science and Technology, University of Maryland.

The Laboratory for Numerical Analysis is an integral part of the Institute for Physical Science and Technology of the University of Maryland, under the general administration of the Director, Institute for Physical Science and Technology. It has the following goals:

- To conduct research in the mathematical theory and computational implementation of numerical analysis and related topics, with emphasis on the numerical treatment of linear and nonlinear differential equations and problems in linear and nonlinear algebra.
- To help bridge gaps between computational directions in engineering, physics, etc. and those in the mathematical community.
- To provide a limited consulting service in all areas of numerical mathematics to the University as a whole, and also to government agencies and industries in the State of Maryland and the Washington Metropolitan area.
- To assist with the education of numerical analysts, especially at the postdoctoral level, in conjunction with the Interdisciplinary Applied Mathematics Program and the programs of the Mathematics and Computer Science Departments. This includes active collaboration with government agencies such as the National Bureau of Standards.
- To be an international center of study and research for foreign students in numerical mathematics who are supported by foreign governments or exchange agencies (Fulbright, etc.).

Further information may be obtained from Professor I. Babuška, Chairman, Laboratory for Numerical Analysis, Institute for Physical Science and Technology, University of Maryland, College Park, Maryland 20742.

**END**

**FILMED**

**7-83**

**DTIC**